Version of Record: https://www.sciencedirect.com/science/article/pii/S1385894721009359
Manuscript_5500134224a66379d7822b312d7d722e

Assessment of a detailed biomass pyrolysis kinetic scheme in multiscale simulations of a single-particle pyrolyzer and a pilot-scale entrained flow pyrolyzer

Xi Gao[1, 2*], Liqiang Lu[1, 2], Mehrdad Shahnam[1], William A. Rogers[1], Kristin Smith[3], Katherine Gaston[3], David Robichaud[3], M. Brennan Pecha[3], Meagan Crowley[3], Peter N. Ciesielski[3], Paulo Debiagi[4], Tiziano Faravelli[5], Gavin Wiggins[6], Charles E.A. Finney[6], James E Parks II[6]

1. National Energy Technology Laboratory, Morgantown, WV 26506, USA

2. Leidos Research Support Team, Morgantown, WV 26506, USA

3. National Renewable Energy Laboratory, Golden, CO 80401, USA

4. Simulation of Reactive Thermo-Fluid Systems, TU Darmstadt, 64285 Darmstadt, Germany.

5. Department of Chemistry, Materials, and Chemical Engineering, Politecnico di Milano, Milan 20133, Italy

6. Oak Ridge National Laboratory, Oak Ridge, Tennessee 37831, USA

** Corresponding author: xi.gao@netl.doe.gov (X. Gao), Tel.: +1 304 285 0989*

Abstract

A detailed biomass pyrolysis kinetic scheme was assessed in the multiscale simulations of a single-particle pyrolyzer with slow pyrolysis and a pilot-scale entrained flow pyrolyzer with fast pyrolysis. The detailed kinetic scheme of biomass pyrolysis developed by the CRECK group consists of 32 reactions and 58 species. A multiscale simulation model was developed, where the CRECK kinetics was employed to simulate biomass pyrolysis reactions, a one-dimensional particle model was utilized to simulate the intraparticle transport phenomena, and the particle-in-cell (PIC) model was employed to simulate the hydrodynamics. The multiscale model was first applied to simulate a single-particle pyrolysis experiment. The simulation with nonisothermal particles matched the experimental data better than the simulation with isothermal particles. Then the multiscale model was applied to simulate the pilot-scale entrained flow pyrolyzer. In this case, the simulation with isothermal particles matched the experimental data better than the simulation with nonisothermal particles. The reason for this difference might be that the kinetics itself already partially included the intraparticle transport effect as it was fitted using both TGA data (slow pyrolysis of small size biomass) and fluidized bed data (fast pyrolysis of relatively large size biomass). This study provides some insights into biomass pyrolysis kinetics development and pyrolyzer multiscale simulation for a future study.

Keywords: Biomass; Pyrolysis; Kinetics; Multiscale; CFD; MFiX

1. Introduction

Pyrolysis of biomass is an efficient technology in the conversion of lignocellulosic feedstocks to value-added fuels and chemicals using external heat under an anoxic or low-oxygen gaseous environment [1-3]. Biomass from a variety of sources, like forest and agricultural residuals, sewage, municipal waste, and algae, can be pyrolyzed to produce liquid fuels, gases, and carbonaceous solids [4]. In industrial applications, fluidized bed reactors [5-7] and entrained flow reactors [8, 9] are commonly employed as biomass pyrolyzers because of the large processing capability and excellent interphase heat transfer. A biomass pyrolysis reactor is a complex multiphase system consisting of reacting gas and solid phases, and also a multiscale system with transport phenomena occurring at the molecular, tissue scale, particle, and reactor scales [10, 11] (see Figure 1). A suitable model accounting for this multiphase, multiscale system is required for pyrolyzer design, optimization, and scale-up.

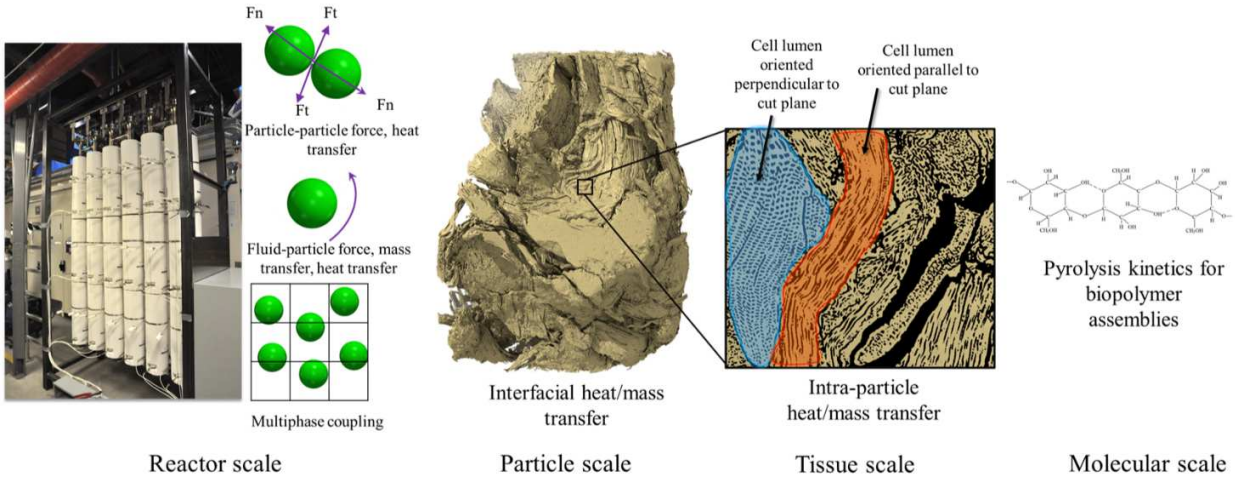

Figure 1. A multiscale simulation framework for a biomass pyrolyzer by integrating a detailed pyrolysis kinetic mechanism, a particle-scale model, and a reactor-scale model.

One of the primary challenges in biomass pyrolyzer simulations is accurately capturing the

molecular conversion kinetics. The complex composition and variability of biomass feedstocks make the pyrolysis reactions extremely complex [12]. Many kinetic schemes have been developed in the literature, ranging from a scheme with only one reaction to complex reaction networks with thousands of reactions [13-15]. Based on the level of complexity, the kinetics can be roughly divided into mechanistic kinetics [16] and lumped kinetics [17]. Mechanistic models describe the detailed mechanism of biomass pyrolysis and include all elementary reactions and possible species. These models are usually beyond the capability of computational fluid dynamics (CFD) solvers due to the stiffness of the fast reactions and are difficult to apply to large-scale reactor simulations. Lumped kinetics models are much simpler than the mechanistic models, where similar species are lumped together as a pseudo species, which is suitable for coupling with the reactor-scale model. In recent years, some detailed lumped biomass kinetic mechanisms with tens of reactions and species were developed [13, 18-20], which are more general than the extremely simplified one-step or two-steps kinetics and provides some flexibilities for modeling different kinds of biomass feedstocks. For example, Debiagi et al. [21] developed a kinetic mechanism (CRECK-S-1805-Bio) with 32 reactions and 58 species using 80 samples of TGA data and fluidized bed data, which can predict the variability of biomass compositions on the products [22] by tuning and adaptation to specific reactor operations.

In most pyrolyzer simulations reported in the literature, the biomass particles were modeled as isothermal, where the temperature was assumed uniform inside a biomass particle. The assumption is valid when the kinetics already consider the intraparticle transport effect or when the particle size is small enough that the intraparticle transport limitation is negligible. In a practical pyrolysis reactor, the biomass particle size is in the range of millimeters to centimeters. Mettler et al. [23] reported that the convection, conduction, and reaction rates are all within an order of

magnitude of one another for a biomass particle with a diameter in the range of 100-1000 microns in a fluidized bed, thus the biomass particles usually can not be assumed isothermal. Particle-resolved simulations [24-26] have been used to study the effect of intraparticle transport phenomena on the biomass pyrolysis products; however, it is extremely expensive to simulate millions of resolved particles in a practical reactor. Lu et al. [27] proposed an offline model to couple the particle-resolved simulations with the reactor model by adding correction factors to the gas-solid heat-transfer and chemical reaction rates. Some studies [28] reported simulations by coupling a one-dimensional particle model with a reactor model for biomass pyrolysis. Gao et al.[29] developed a multiscale model by integrating a simple biomass pyrolysis kinetics, a particle-scale model, and a shape-resolved SuperDEM-CFD model[30, 31] for biomass pyrolyzer simulation. However, a multiscale simulation by integrating a detailed kinetics mechanism, a particle-scale model, and a reactor model was seldom reported in the literature.

The study is organized as follows. In section 2, the detailed kinetic mechanism developed by Debiagi et al. [21] and a 1-D particle model was implemented in the open-source CFD suite MFiX[32]. In section 3, the experiment and modeling setting was introduced. In section 4, the multiscale model was applied to simulate a single-particle pyrolyzer and a pilot-scale entrained flow reactor. The simulation using both the isothermal model and nonisothermal model was compared with the experimental data to explore the advantages and limitations of the CRECK kinetics were discussed. The kinetic model was developed in previous work [21] and applied for a fluidized bed simulation[33], however, the literature still lacks studies evaluating the performance of this kinetic model for more complex reacting systems, in which transport phenomena must be considered. Thus, the novelty of this study is the employment and extrapolation of the CRECK biomass pyrolysis model for complex systems, validating its extended applicability. This work

opens a path for implementing this model for the design and improvement of industrial-scale pyrolyzers, gasifiers, and combustors.

2. Methods

2.1. Detailed pyrolysis kinetic mechanism

A detailed biomass pyrolysis kinetic mechanism developed recently by Debiagi et al. [21] was employed in this study. The kinetics include 32 chemical reactions, 29 solid species, and 29 gas species. The multistep multicomponent kinetics treat the biomass pyrolysis as a combination of the decomposition of cellulose (CELL; reactions 1-4), hemicellulose (GMSW, XYHW, XYGR; reactions 5-10), lignin (LIG-C, LIG-O, LIG-H; reactions 11-18), and extractives (TANN, TGL; reactions 19-21). The mass fractions of cellulose, hemicellulose, lignin, extractives, moisture, and ash in the biomass particles are required as inputs to the kinetics, and these are usually obtained by experimental measurement or estimation using a characterization procedure that requires only the ultimate analysis [12]. The products include condensible bio-oil (22 species), bio-gas (6 species), water, and biochar. The bio-oil contains a large number of polycyclic aromatic hydrocarbons (PAHs) and oxygenates with more than 6 carbon atoms, which was reflected by the species VANILLIN ($C_8H_8O_3$), CRESOL(C_7H_8O), HMWL ($C_{24}H_{28}O_4$), MLINO($C_{19}H_{34}O_2$), U2ME12($C_{13}H_{22}O_2$). The biochar is considered as the sum of all solid residues, including pure carbon, metaplastic species, and ash. The mass fraction of metaplastic in the biochar depends on the biomass residence time in the pyrolyzer, as the “trapped” gases are slowly released from the metaplastics (reaction 22-31). Both TGA data and fluidized-bed pyrolyzer data were used to develop the kinetics. The intraparticle transport effect is minimal in the TGA data (small size particles, slow pyrolysis (residence time in the order of minutes or hours)), while the intraparticle transport effect might exist in the fluidized bed data (relatively large size particles, fast pyrolysis). The CRECK kinetics thus partially includes the intraparticle transport. A schematic description of

the CRECK kinetics is shown in Figure 2. Detailed reactions and kinetic parameters are provided in the supplemental materials. The advantage of the model developed by Debiagi et al. can be summarized as (1) the model was developed using 80 samples of data with different biomass types and operating conditions, which is a general kinetics model when compared with other kinetics models for a specific biomass type and condition. (2) the kinetics includes 32 reactions and 58 species, which can provide more details than the extremely simplified kinetics with only several reactions and species. Also, the model uses a CHEMKIN-like format to express the kinetic constants, which allow a straightforward coupling with CFD for pyrolyzer simulation. Mechanistic models, containing hundreds of species and thousands of reactions, are still not suitable for reactor scale simulation.

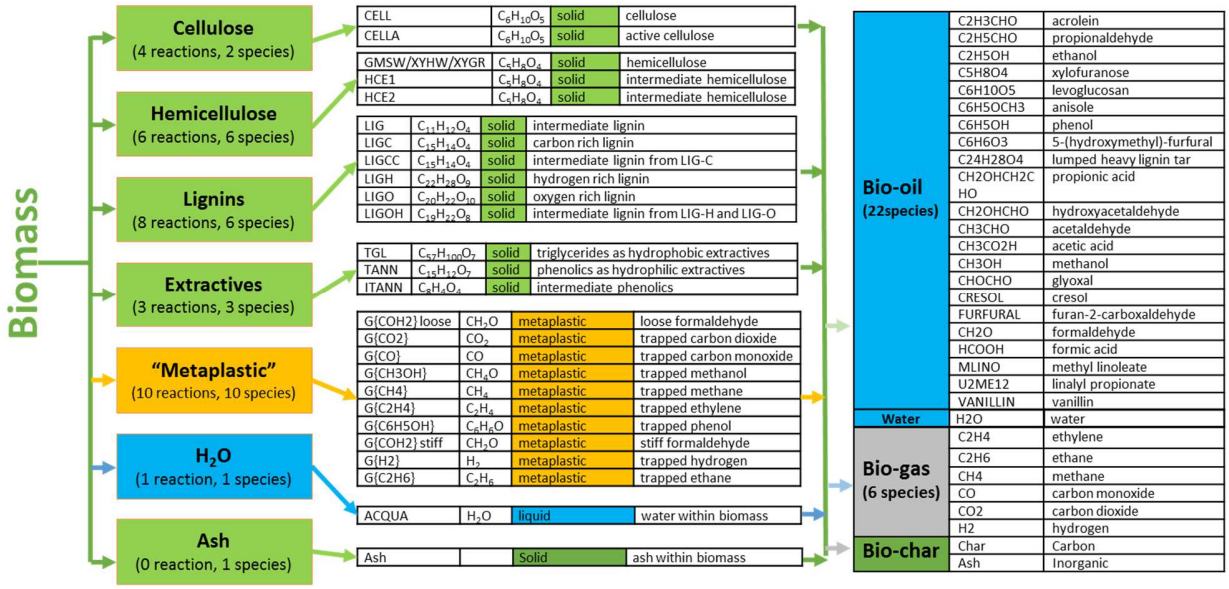

Figure 2. An illustration of the detailed biomass pyrolysis kinetics reported by Debiagi et al. [21]. (The same color was used for species with similar properties.)

2.2. Particle-scale model

The intraparticle transport was modeled using a transient 1-D particle-scale model with

chemical reactions and heat transfer. A general form of the 1-D temperature equation ($b=2$, sphere; b=1, long cylinder; $b=0$, long plate) can be expressed as follows:

$$\frac{\partial}{\partial t}\left(\rho_s c_{p,s} T_s\right) = \frac{1}{r^b}\frac{\partial}{\partial r}\left(k_s r^b \frac{\partial T_s}{\partial r}\right) + \sum\left(-\Delta H_i R_i\right) \quad (1)$$

Where ρ_s is the instantaneous particle density, $c_{p,s}$ is the particle thermal capacity, k_s is the particle thermal conductivity, ΔH_i is the heat of reaction i, and R_i is the reaction rate.

The boundary conditions are:

$$\left.\frac{\partial T_s}{\partial r}\right|_{r=0} = 0 \quad (2)$$

$$k_s \left.\frac{\partial T_s}{\partial r}\right|_{r=r_0} = h_{gs}(T_f - T_s) \quad (3)$$

Where h_{gs} is the gas–particle heat transfer coefficient.

The solid species transport equations are expressed as:

$$\frac{dX_{i,s}}{dt} = \sum R_i \quad (4)$$

Where $X_{i,s}$ is the solid species.

Eqs. (1-3) were discretized using a finite-difference scheme and were converted into the matrix form $\boldsymbol{A}\cdot\boldsymbol{T}=\boldsymbol{B}$, where $\boldsymbol{A}$ is a tridiagonal matrix, $\boldsymbol{T}$ is the unknown temperature vector, $\boldsymbol{B}$ is the vector as a function of known temperature and species. The 1-D particle model was solved using a tridiagonal matrix algorithm in MFiX.

2.3. Particle phase

The position and trajectory of solid particles were tracked by Newton's laws in the Lagrangian framework using the particle-in-cell (PIC) model [34, 35], where several particles were lumped together as a computational parcel to speed the simulation. In each computational parcel, the particles have the same properties and boundary conditions. Different from the discrete element method (DEM) [36, 37] but similar with the two-fluid model [38], the particle–particle interaction in PIC is modeled using a continuum stress model instead of particle–particle collision force. The governing equations for the parcel position and velocities can be expressed as:

$$\frac{d\boldsymbol{X}_p}{dt} = \boldsymbol{U}_p \tag{5}$$

$$W_p m_p \frac{d\boldsymbol{U}_p}{dt} = W_p (m_p \boldsymbol{g} + \mathbf{F}_{\text{g-p}} + \mathbf{F}_{\text{p-p}}) \tag{6}$$

Where m_p, $\boldsymbol{U}_p$ and W_p are the particle mass, translational velocity, and statistical weight (number of particles in a parcel), respectively. $\mathbf{F}_{\text{g-p}}$ and $\mathbf{F}_{\text{p-p}}$ are fluid–particle force and particle–particle force [39], respectively and can be expressed as follows:

$$\mathbf{F}_{\text{g-p}} = \frac{\pi}{6} d_{\text{p}}^3 \left(\frac{\beta(\mathbf{u}_{\text{g}} - \mathbf{u}_{\text{p}})}{1-\varepsilon_{\text{g}}} - \nabla P_{\text{g}}\right) \tag{7}$$

$$\mathbf{F}_{\text{p-p}} = -\frac{\pi d_{\text{p}}^{\ 3}}{6\varepsilon_{\text{s}}} \nabla \tau_{\text{s}} \tag{8}$$

$$\tau_{\text{s}} = \frac{P_{\text{s}} \varepsilon_{\text{s}}^{\theta}}{\max[\varepsilon_{\text{s,cp}} - \varepsilon_{\text{s}}, \delta(1-\varepsilon_{\text{s}})]} \tag{9}$$

Where τ_s is the particle–particle stress, $\varepsilon_{s,cp}$ is the solid volume fraction at close packing, P_s is the particle pressure, θ is a dimensionless parameter, and δ is a constant to assure a non-zero denominator in calculation. The default values of the parameters were used in the simulation [34].

The species and energy conservation equations can be expressed as:

$$\frac{d(W_p m_p X_{i,p})}{dt} = W_p R_{i,p}$$

(10)

$$W_p m_p C_p \frac{dT_p}{dt} = W_p Q_{p,conv} + W_p Q_{p,reaction} \quad (11)$$

Where C_p, T_p are the particle specific heat and particle (same for parcel) temperature, respectively. $Q_{p,conv}$ is particle–fluid heat transfer rate, and $Q_{p,reaction}$ is the heat generation due to chemical reactions.

In this study, a variable particle density model (shrinking density) was employed instead of a variable particle diameter model, which is widely adopted in the literature for biomass particle pyrolysis. A variable particle density and particle diameter model should be used to model the real biomass particle pyrolysis process, however, this will make the model extremely complex, especially when coupled with the particle scale model.

2.4. Gas phase

The gas phase is modeled by the Navier–Stokes equations and solved using the finite volume method. The gas-phase mass and momentum equations can be expressed as:

$$\frac{\partial(\varepsilon_g \rho_g)}{\partial t} + \nabla \cdot (\varepsilon_g \rho_g \boldsymbol{u}_g) = R_g \quad (12)$$

$$\frac{\partial(\varepsilon_g \rho_g \mathbf{u}_g)}{\partial t} + \nabla \cdot (\varepsilon_g \rho_g \mathbf{u}_g \mathbf{u}_g) = -\varepsilon_g \nabla P + \varepsilon_g \nabla \cdot \boldsymbol{\tau}_g + \varepsilon_g \rho_g \mathbf{g} - \mathbf{I}_{drag} \quad (13)$$

Where ε_g, ρ_g and $\mathbf{u}_g$ are the gas voidage, gas density, and gas velocity, respectively. P, $\boldsymbol{\tau}_g$ are the gas pressure and stress tensor. $\mathbf{I}_{drag}$ is the drag force between gas–solid phase. R_g is the mass source term due to chemical reactions.

The gas-phase species and energy balance equations can be expressed as:

$$\frac{\partial(\varepsilon_g \rho_g X_{i,g})}{\partial t} + \nabla \cdot (\varepsilon_g \rho_g \mathbf{u}_g X_{i,g}) = \nabla \cdot (D_i \nabla X_i) + R_g^i + S_{X_i}$$

(14)

$$\varepsilon_g \rho_g C_{p,g} \left(\frac{\partial T_g}{\partial t} + \mathbf{u}_g \cdot \nabla T_g\right) = -\nabla \cdot \mathbf{q}_g + \mathbf{I}_{heat} - Q_{g,\,reactions}$$

(15)

Where $X_{i,g}$ D_i, $C_{p,g}$ gas species mass fraction,diffusion coefficient, heat capacity, respectively. is the heat transfer between gas and solid phases. the source term for species *i* due to chemical reactions, and $Q_{g,reaction}$ is the heat generated by chemical reactions.

2.5. Drag law

The Ganser drag coefficient [40] coupled with the Defelice drag model [41] was employed to calculate the drag force on cylindrical biomass particles. The Ganser drag coefficient was validated in previous work, which showed excellent prediction for cylindrical biomass particles [31, 42]. The drag model can be expressed as:

$$\beta_j = \frac{3}{4} \frac{\varepsilon_g \left(1-\varepsilon_g\right) \rho_g \left|\boldsymbol{u}_g - \boldsymbol{u}_{p,j}\right|}{d_p} C_{D0}\, \varepsilon_g^{\,1-\chi}$$

(16)

$$\chi = 3.7 - 0.65 \exp\left(-\frac{(1.5-\log Re)^2}{2}\right)$$

(17)

$$C_{\mathrm{D0}}^{Ganser} = \frac{24}{\mathrm{Re}_p K_1}(1+0.1118(\mathrm{Re}_p K_1 K_2)^{0.6567}) + \frac{0.4305 K_2}{1+3305/(\mathrm{Re}_p K_1 K_2)}$$

(18)

$$K_1 = (\frac{1}{3}+\frac{2}{3}\varphi^{-0.5})^{-1} - 2.25\frac{d_p}{D}$$

(19)

$$K_2 = 10^{1.8148(-\log\phi)^{0.5743}}$$

(20)

Where φ is the sphericity of the particle, d_p is the volume equivalent sphere diameter, β_j is the drag force on particle j, $\boldsymbol{u}_{\mathrm{pj}}$ is the velocity of particle j, and D is the diameter of the fluidized bed.

2.6. Gas–solid heat transfer model

The gas–solid heat transfer coefficient can be calculated as :

$$h_{conv} = \frac{\mathrm{Nu}}{k_g d_e}$$

(21)

Where k_g is the gas thermal conductivity, Nu is the particle Nusselt number, and d_e is the characteristic length, and is determined by the diameter of the cylindrical particle. Tavassoli et al. [43] reported a modified Gunn correlation [44] that can reasonably well predict the heat transfer of rod-like particles in fixed beds and fluidized beds. The correlation of Nusselt number is expressed as:

$$\mathrm{Nu} = (7-10\varepsilon_g+5\varepsilon_g^2)(1.0+0.1\mathrm{Re}^{0.2}\,\mathrm{Pr}^{1/3}) + (1.33-2.19\varepsilon_g+1.15\varepsilon_g^2)\mathrm{Re}^{0.7}\,\mathrm{Pr}^{1/3}$$

(22)

3. Experiment and modeling setups

3.1. Single-particle biomass pyrolysis experiment and modeling setups

The single-particle biomass pyrolysis experiment reported by Anca–Couce et al. [45] was employed as a test case, where a cylindrical spruce biomass particle (8 mm diameter and 19 mm length) was pyrolyzed in a small-scale reactor with a diameter of 50 mm, which is placed an electrically heated oven. Hot nitrogen was injected from the bottom of the tube to pyrolysis the biomass particle. The particle center and surface temperatures were measured using a Type N thermocouples. The product compositions of the online release of volatiles were measured with a multi-component Fourier transform infrared (FTIR) spectroscopy devise and recorded at a frequency of 2 seconds. The time delays are in the order of milliseconds and are negligible in the experiment. Detailed experimental results were reported, including the instantaneous particle surface and center temperature, the instantaneous residue mass faction (biochar), and the instantaneous release of major species, like the condensable organics, CO, CO_2, and water. The particle properties are summarized in Table 1.

Table 1. Spruce biomass particle properties and parameters used in the particle-scale model [45].

Parameter	**Value**
Diameter [mm]	8
Length [mm]	19
Particle density [kg/m^3] (wet basis)	1217.4
Biomass thermal conductivity [W/(m·K)]	0.056+0.00026T
Biochar thermal conductivity [W/(m·K)]	0.125
Ash thermal conductivity [W/(m·K)]	0.14
Moisture thermal conductivity [W/(m·K)]	0.61
Particle initial temperature [K]	300
Gas temperature [K]	823
Moisture (wet basis)	0.08
Ash (dry basis)	0.004
Carbon (dry basis, ash-free)	0.5015

Hydrogen (dry basis, ash-free)	0.0623
Cellulose (dry basis, ash-free)	0.44
Hemicellulose (GMSW) (dry basis, ash-free)	0.26
Lignin (LIG-C) (dry basis, ash-free)	0.175
Lignin (LIG-H) (dry basis, ash-free)	0.095
Lignin (LIG-O) (dry basis, ash-free)	0.03

3.2. Pilot-scale entrained flow pyrolyzer experiment and modeling setups

As a larger-scale test case, experiments were conducted in the pilot-scale entrained flow reactor within the Thermal and Catalytic Process Development Unit (TCPDU) at the National Renewable Energy Laboratory (NREL). The TCPDU consists of biomass feed transport systems, an entrained flow pyrolysis reactor, solids removal and collection systems, liquid condensation, filtration, and collection systems, and biomass vapor-phase upgrading systems [46, 47]. This study only focused on the simulation of the entrained flow reactor (EFR). The schematic geometry of EFR for biomass pyrolysis is shown in Figure 3. The EFR is a folded riser with six parallel loops. The inner diameter of the tube is 0.0381 m, and the height is 2.25 m. A low-cost biomass mixture (called Blend3) of 60% air-classified forest residues, 30% clean pine and 10% hybrid poplar was fed into the reactor at a mass flow rate of 15 kg/h. The biomass mixture used in this study is used to mimic the waste biomass with a very low collecting cost that can be used in an industrial-scale reactor. The reactor wall temperature was maintained at 500 °C by using external heating jackets, and the pressure was controlled at 142.5 kPa. Hot nitrogen gas at 500 °C was used to entrain the biomass particles into the pyrolyzer. The produced biogas, bio-oil, water, and biochar at the reactor outlet were collected and analyzed [48]. The biomass particle properties and numerical parameters are summarized in Table 2. The biomass's physical properties were characterized at the National Energy Technology Laboratory (NETL), whereas the proximate and ultimate analysis and the biomass component analysis (mass fraction) were measured at NREL.

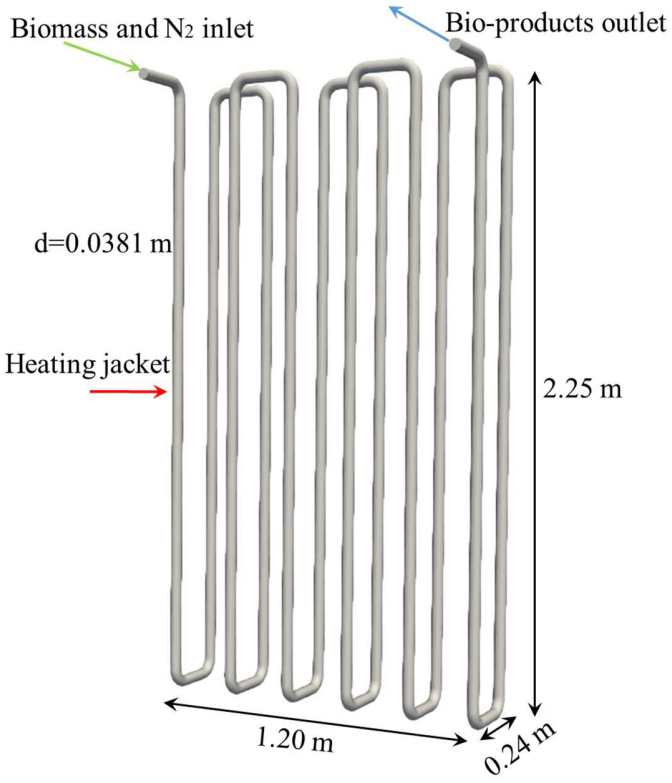

Figure 3. Schematic geometry of the entrained flow reactor.

Table 2. Physical properties, proximate, ultimate analysis, and composition analysis of Blend3 biomass used in the pilot-scale EFR.

Parameter	**Value**
Cylinder: Length/diameter ratio	5
Volume equivalent sphere diameter [μm], 7 bins	140, 362, 600, 838, 1076, 1314, 1791
Mass fraction in each bin, 7 bins	0.293, 0.250, 0.231, 0.138, 0.056, 0.023, 0.009
Particle density [kg/m^3] (wet basis)	703.0
Parcel–wall restitution coefficient	0.1
Statistic weight, W_p [-]	50
Volatiles (wet basis)	0.7640
Fixed carbon (wet basis)	0.1692
Moisture (wet basis)	0.0604
Ash (wet basis)	0.0064
Carbon (dry basis, ash-free)	0.5306
Hydrogen (dry basis, ash-free)	0.0566
Oxygen (dry basis, ash-free)	0.4110
Nitrogen (dry basis, ash-free)	0.0016

Sulfur (dry basis, ash-free)	0.0002
Cellulose (dry basis, ash-free)	0.3918
Hemicellulose (GMSW) (dry basis, ash-free)	0.2471
Lignin (LIG-H) (dry basis, ash-free)	0.1820
Lignin (LIG-O) (dry basis, ash-free)	0.1148
Extractive (TGL) (dry basis, ash-free)	0.0643

3.3. Numerical method

The CRECK kinetics and 1-D particle model were implemented in the open-source CFD suite MFiX [32, 49] developed at NETL. MFiX-PIC solver coupled with the fluid solver was employed to simulate the hydrodynamics and chemical reactions in the pyrolyzer. The pressure–velocity coupling was solved using the Semi-Implicit Method for Pressure Linked Equations (SIMPLE), and a second-order upwind scheme was employed for the fluid solver. At the inlet, a mass inflow boundary was set and at the outlet, a pressure outlet boundary was set. At the wall, a no-slip wall boundary was used for the fluid. A cut-cell technique was used for the modeling of complex geometry [50]. The cell size used in the simulation is $0.0067 \times 0.0067 \times 0.0067$ m^3, which makes the cell size 1.02 times the largest parcel diameter. A variable time step scheme was used with the time step between 1.0×10^{-5} – 1.0×10^{-2} s. For the EFR simulation, 1200 CPU threads were used, and 40 seconds simulation of each case were conducted on the Joule 2 supercomputer at NETL. The computational cost is 2.625 seconds/day (physical time/wall clock time) for the isothermal model and 1.075 seconds/day for the nonisothermal model.

4. Results and discussion

4.1. Single-particle pyrolyzer simulation

Figure 4 shows the comparison of the predicted center and surface temperature evolution with time with the experimental data. The single-particle pyrolysis experiment took about 175 seconds

to reach the pyrolysis temperature, which is slow pyrolysis. The center temperature of the particle doesn't reach 800 K until around 180 seconds, while the surroundings are maintained at a constant temperature. Meanwhile, the bulk of mass loss due to pyrolysis has already occurred by that time, indicating that pyrolysis begins around the time that the exterior of the particle reaches 700 K, with the center still below 500 K. While the exterior layers heat faster, reacting at higher temperatures, the core has a slower heating profile and the conversion takes place at lower temperatures, shifting the selectivity to different reacting paths. Therefore, significant differences in product distribution could take place when comparing the core and the more external layers, indicating even higher differences for larger particle sizes. The difference between the center and surface temperatures reached up to 200 K, which indicated a significantly non-uniform temperature distribution inside the biomass particle. The predicted temperature profiles agree well with the experimental data, which shows that the CRECK kinetics coupled with the 1-D particle model can correctly simulate the single-particle biomass particle pyrolysis. To quantify the accuracy of the model, the related errors were calculated as follows:

$$E_{abs} = \frac{\sum_{i=1}^{N} \left| T_{sim}^{i} - T_{\exp}^{i} \right|}{\sum_{i=1}^{N} T_{\exp}^{i}}$$

(23)

Where N (=70) is the number of points used in the calculation. The related errors for surface and center temperature prediction are 3.1%, 5.2%, respectively. Simulations with isothermal and nonisothermal models were compared in Figure 4(b) and Figure 5. The isothermal particle model predicted larger volume-averaged temperature and overpredicted the reaction rates, which shows that the isothermal model widely used in the literature could lead to substantial errors. Figure 5(b) shows the comparison of predicted residual mass fraction using isothermal and nonisothermal

particle models at different particle sizes (other modeling parameters remain unchanged) in the single-particle pyrolyzer. It can be seen that with the decrease of cylinder diameter, the difference between the isothermal particle and non-isothermal particle becomes less significant. When the cylinder diameter is less than 1000 microns, the effect of intraparticle transport can be neglected for slow pyrolysis.

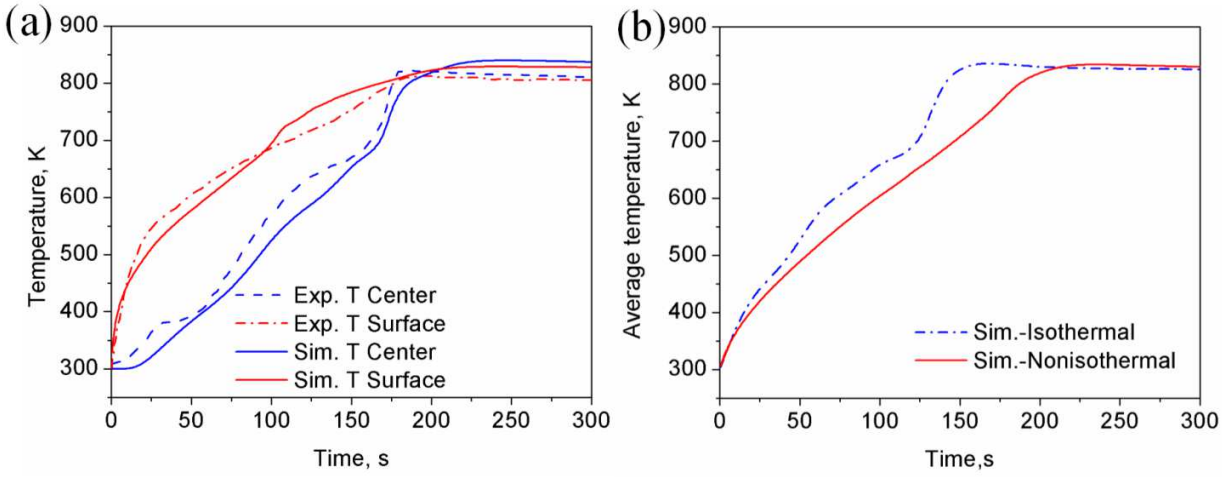

Figure 4. (a). Comparison of predicted center and surface temperature with experimental data using nonisothermal particle model, (b) comparison of predicted average temperature using the isothermal and nonisothermal model.

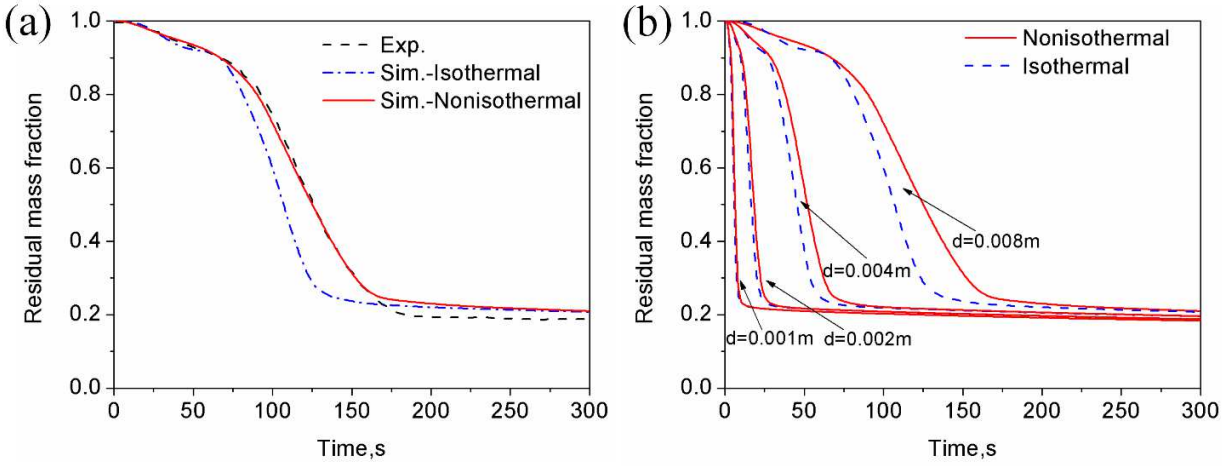

Figure 5. (a) Comparison of predicted residual mass fraction using isothermal and nonisothermal particle model with experimental data. (b) Effect of cylinder diameter on intraparticle transport.

The comparison of simulated product distribution with experimental data is shown in Figure 6. The product mass fractions were not significantly affected by the temperature gradient inside the particle, and the final mass fractions of biochar, bio-gas, bio-oil (water-free), and water predicted by both models were very similar. This is because the residence time is sufficiently long, all the volatile matter in biomass was released, including the pyrolysis of extractives and metaplastic, which have relatively low reaction rates. The endothermic nature of biomass components is clearly observed in Figure 4, for example in 125-150 s, where the cellulose is decomposed releasing large amounts of tars (mostly levoglucosan). The heat of evaporation of this species is very high which drives the overall endothermic profile at such temperatures. Also observed by other authors [22], a core temperature overshooting takes place at around 180s, when some exothermic char forming reactions take place (and relatively low conductivity), typically after the decomposition of most of the biomass initial components.

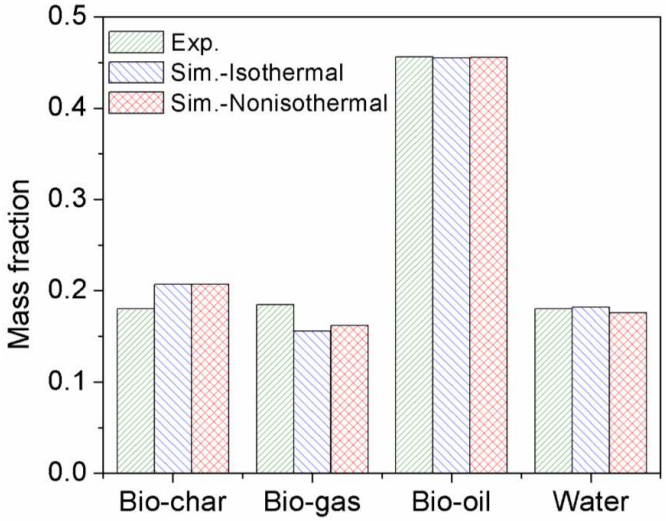

Figure 6. Comparison of the predicted main product mass fractions using the isothermal and nonisothermal models with the experimental data.

To further compare the isothermal and nonisothermal models, the instantaneous release of major products, like condensable organics, H_2O, CO, and CO_2, were compared and shown in Figure 7. The predicted results by the nonisothermal model indeed match better with the experimental data. The species release rate predicted by the isothermal model is faster, which is consistent with the previous analysis. More comparisons between models and experiments were summarized in Table 5, including elemental analysis in the biochar, gas species in the gas phase, and major species in the bio-oil. Note that, when the system has a hot atmosphere (above 800 K), the volatiles released from the particle faces severe conditions, which lead to secondary-gas phase reactions including the tar-cracking process, shifting the distribution of products into more light gases and less heavy tars. The effect of gas-phase reactions, which is the objective of future investigations, when detailed gas-phase kinetics will be coupled for further analysis.

Table 3. Comparison of predicted product compositions in mass percentage.

Items or names	**Experiment**	**Simulation - Isothermal**	**Simulation-Nonisothermal**
Bio-char	0.180±0.004	0.2068	0.2070
C in biochar	0.8464	0.7837	0.7837
H in biochar	0.0314	0.0440	0.0440
O in biochar	NA	0.1500	0.1500
ash in biochar	0.0179	0.0222	0.0222
Bio-gas	0.185±0.005	0.1560	0.1621
CO	0.048±0.001	0.0627	0.0636
CO_2	0.116±0.004	0.0684	0.0669
CH_4	0.015±0.000	0.0105	0.0097
H_2	NA	0.0015	0.0014
Other light gases	0.006±0.000	0.0129	0.0205
Bio-oil (light + heavy)	0.456±0.006	0.4552	0.4553
Formaldehyde (CH_2O)	0.015±0.001	0.0138	0.0138
Acetic acid ($C_2H_4O_2$)	0.037±0.001	0.0346	0.0350
Hydroxyacetaldehyde ($C_2H_4O_2$)	NA	0.0088	0.0094
Methanol (CH_3OH)	0.007±0.000	0.0194	0.0209
Ethanol (C_2H_6O)	0.071±0.001	0.0012	0.0011
Formic acid (HCOOH)	NA	0.0028	0.0027

Glyoxal ($C_2H_2O_2$)	NA	0.0072	0.0068
Acetone $C_3H_6O_2$)	NA	0.0276	0.0271
Ethylform ($C_3H_6O_2$)	NA	0.0079	0.0077
Acrolein (C_3H_4O)	NA	0.0013	0.0013
Total light oil (not cyclic oxygenated species)	0.152±0.002	0.1245	0.1260
Levoglucosan ($C_6H_{10}O_5$)	NA	0.1870	0.1865
HMFU ($C_6H_6O_3$)	NA	0.0465	0.0471
Total heavy oil	0.304±0.004	0.3310	0.3293
H_2O	0.180±0.004	0.1821	0.1756
Total	1.00	1.00	1.00

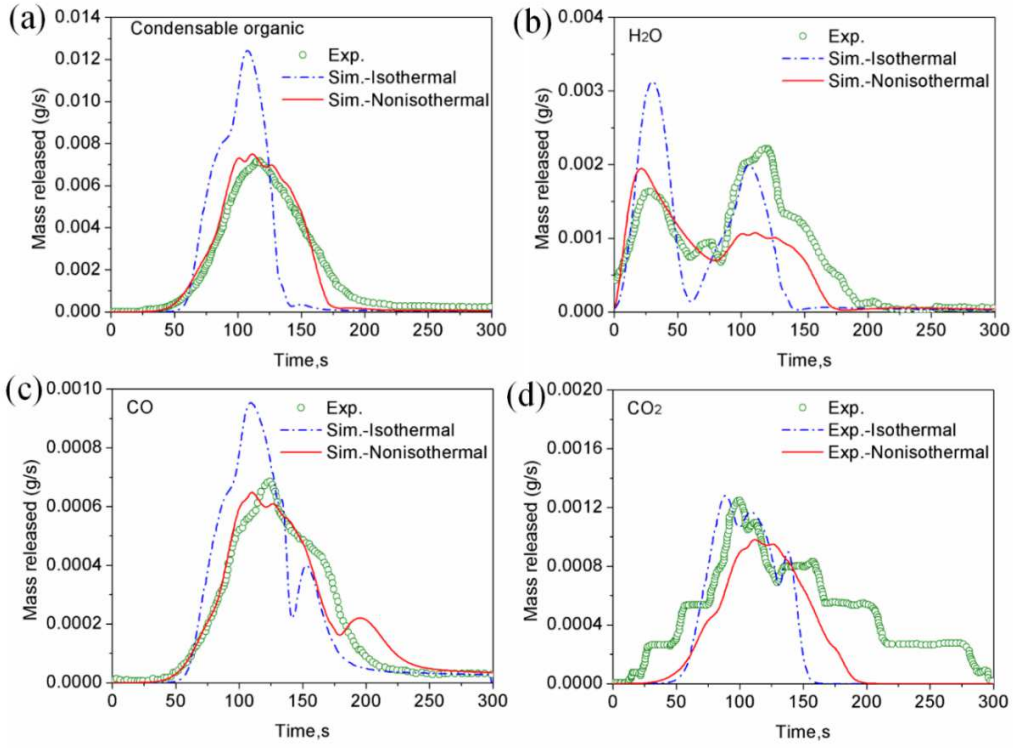

Figure 7. Comparison of the predicted release of major products with the experimental data.

4.2. Pilot-scale EFR simulation

4.2.1. Residence time and residual mass fraction

A snapshot of the parcel size distribution is shown in Figure 8. Non-uniform distribution of

particles can be observed, and the segregation of particles is expected. The mean residence time is calculated as: $RTD_{mean} = \frac{1}{N}\sum_{i=1}^{N} RTD_i$, which is numerical average instead of mass average. The residence time in the reactor is not only affected by the flow hydrodynamics (like velocity, temperature) but also the biomass particles (like size, conversion). Harvested parcels at the reactor outlet were analyzed, and the distribution of residence time and the residual mass fraction (1−conversion) are shown in Figure 9. With the increase of particle size, the residual mass fraction changed slightly. The overall residual mass fraction of biomass particles are affected by the residence time of a particle size class, the mass fraction of a particle size class, and the number fraction of a particle size class. If the residence time is the same for particles of different sizes, the residual mass fraction of larger particles should be larger. However, the residence times of particles of different particle sizes are different, which was mainly affected by the gas-particle interaction, particle-particle interaction, and particle-wall interaction. As can be seen in Figure 9, the residence time of larger particles is larger, which could explain the almost same residual mass fraction for particles of different sizes. The mean residence time predicted by the nonisothermal particle model is about 5.8 s, which is slightly lower than that (8.9 s) predicted by the isothermal particle model. The reason is that, in the isothermal particle model, the strong heat transfer between gas and biomass particles significantly decreases the gas temperature, and thus decreases the gas phase velocity and viscosity. In Figure 9(b), it can also be seen that the residual mass fraction predicted by the nonisothermal model is about 50% larger than that of the isothermal model, which shows that for fast pyrolysis the intraparticle transport effect can not be neglected.

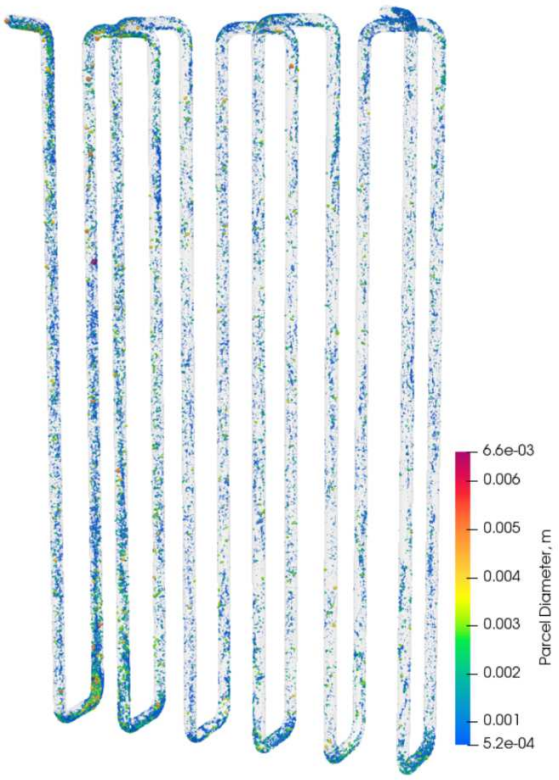

Figure 8. A snapshot of biomass parcels distribution in the EFR reactor.

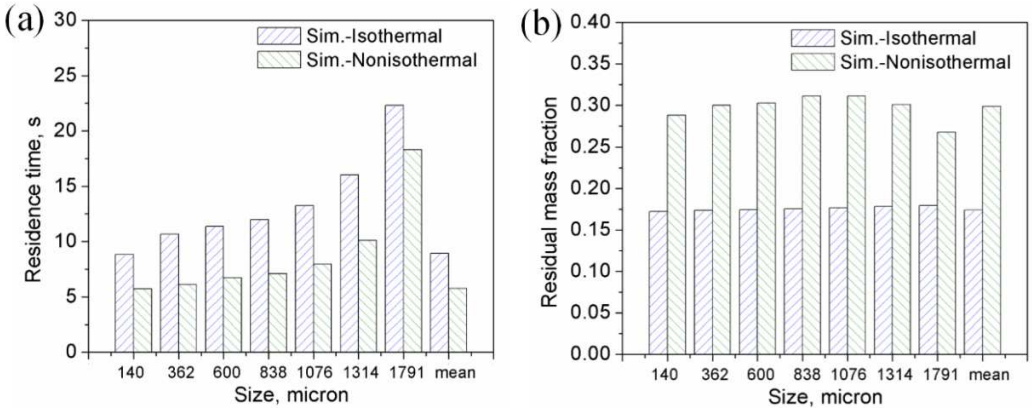

Figure 9. Influence of particle sizes on the residence time and the residual mass fraction.

4.2.2. Products distribution

The yields of biochar, biogas, bio-oil, and water are compared in Figure 10. The comparison of the CHO elemental composition in biochar and bio-gas is shown in Figure 11. The biochar yield in

the experiment and the isothermal and nonisothermal model is 14.2%±0.1%, 17.4%, and 29.1%, respectively. The experiment reported a mass balance of 96.9% ± 1.5 % and a carbon balance of 93.0% ± 1.0 %. Considering the errors in the experimental data, the isothermal model simulation results match well with the experimental data. The comparison of gas species in the bio-gas is listed in Table 4. The isothermal model with detailed CRECK kinetics reasonably well predicted the mass fraction of the major gas species in the bio-gas, like CO, CO_2, and CH_4, even though some errors for the minor gas species (like C_2H_4, C_2H_4) were also observed. Some other gas species (C_3H_6, C_3H_8, C_4H_8) were not available in the kinetics. A comparison of the predicted mass fractions in bio-oil using the isothermal and nonisothermal models is shown in Figure 12. The species distribution by the two models is quite similar. The top two species in the bio-oil by both models are $C_6H_{10}O_5$, $C_6H_6O_3$, which accounts for 45% of all bio-oil. A comparison of the predicted mass fractions in bio-char using the isothermal and nonisothermal models was shown in Figure 13. It can be seen that the species distribution by the two models is quite different. In the isothermal model, the species with the largest mass fraction is char, which accounts for 46.5% of the bio-char. While in the non-isothermal model, the metaplastic species LIGOH has the largest mass fraction (45.3%), which shows that the pyrolysis reaction has not reached the steady-state due to short residence time. This is because the relatively low reaction rate of metaplastic was further reduced when couping with the particle scale model.

In summary, the CRECK kinetics include transport effects when it comes to fast pyrolysis that is not included when it comes to slow pyrolysis. The results of this study indicate that there is no need to consider the intraparticle transport effect when applying the CRECK kinetics for biomass pyrolysis simulation in fluidized beds. It is also possible that the isotropic nature of the 1-D model could suppress heat transfer. Usually, biomass particles are anisotropic[51]. Real pine

particles have permeability in the axial direction which is up to 100,000 times higher than in the radial direction [52]. Therefore, when biomass particles undergo a phase change from solid to gas, it is predominantly released from the ends of the particles and the sides may still receive cross-draft of hot gases, depending on the particle orientation to the gas stream. Thus it is feasible that an isotropic model will underpredict superficial gas velocity/temperature at the sides of the wood particle and thus under-predict heat transfer. The accuracy of the isothermal model could therefore be a compensating effect of predicting faster internal heat transfer and slower surface heat transfer. Note that, biomass feedstock particles used in the EFR were milled, pelletized, and then crushed. This processing results in particle agglomerates that comprise multiple sub-particles in different orientations as shown in the "Particle Scale" and "Tissue Scale" panels of Figure 1. Woody feedstocks that are simply milled contain highly anisotropic intraparticle porosity that originates from the alignment of cell lumen within the wood tissue. This feature causes intraparticle transport phenomena to depart from 1-D approximations for particles larger than ~2 mm[53]; however, the pelletized/crushed feedstock particles used in this study contain multiple domains of essentially randomly oriented internal porosity which mitigates the anisotropic tissue structure typical of milled particles and thereby supports the application of isotropic intraparticle transport model. This topic should be further explored in future work.

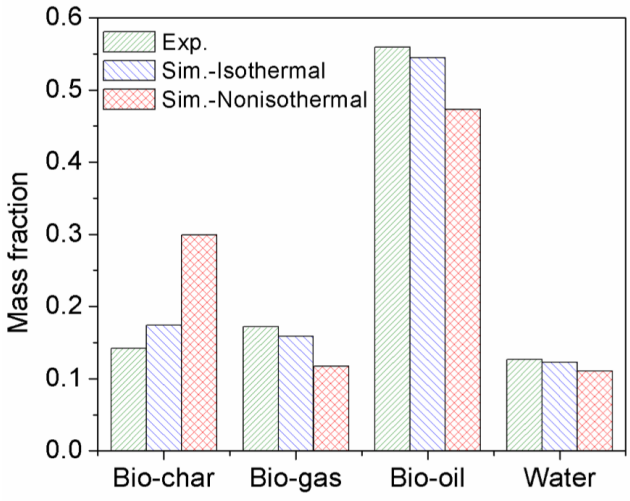

Figure 10. Comparison of predicted product distribution using the isothermal and nonisothermal model with experimental data.

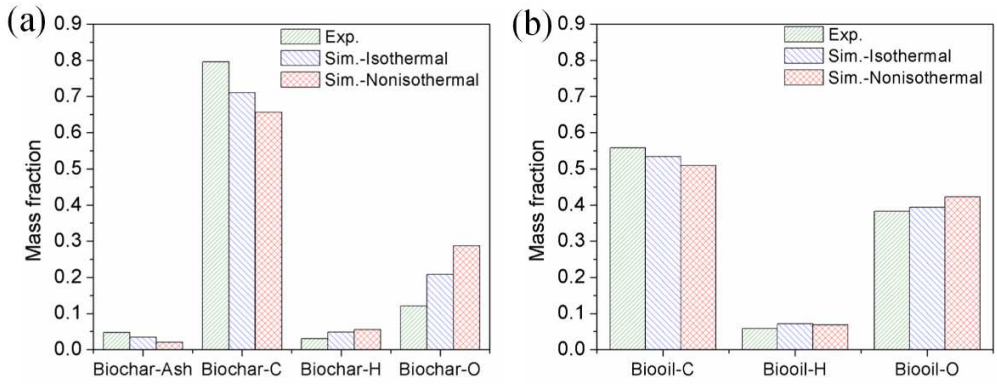

Figure 11. Comparison of predicted element mass fraction in biochar (a) and bio-oil (b) using the isothermal and nonisothermal model with experimental data.

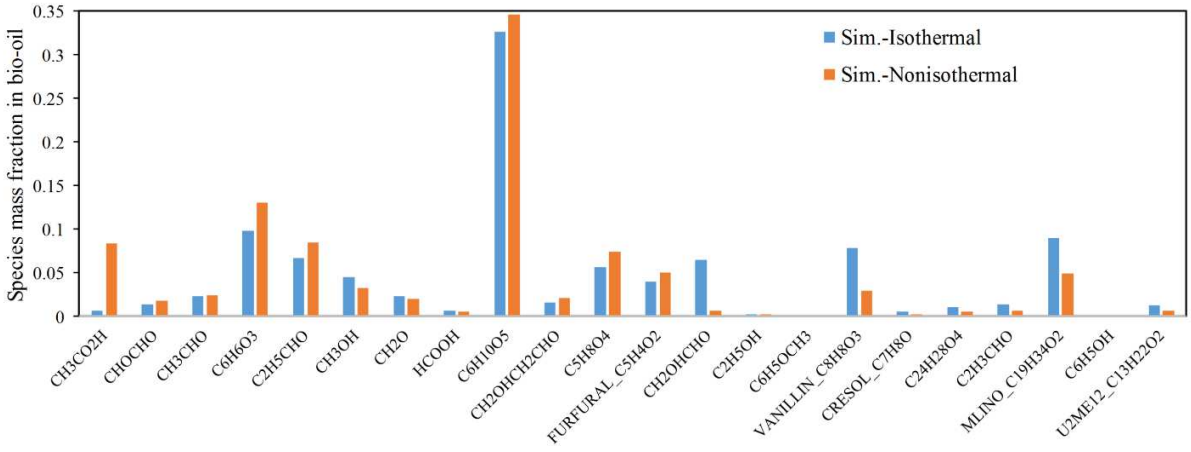

Figure 12. Comparison of the predicted mass fractions in bio-oil using the isothermal and nonisothermal models.

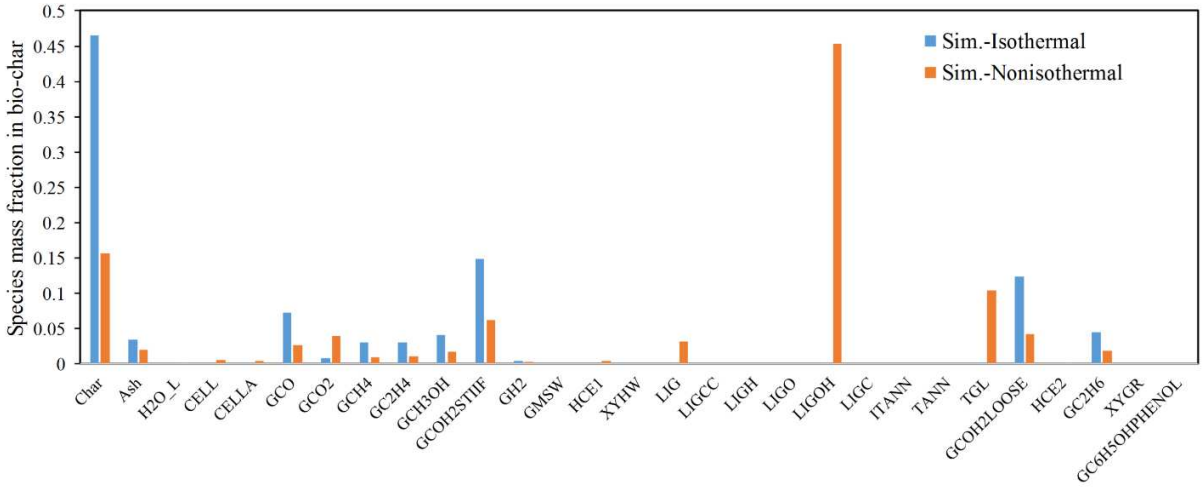

Figure 13. Comparison of the predicted mass fractions in bio-char using the isothermal and nonisothermal models.

Table 4. Comparison of predicted biogas species distribution with the experimental data in the entrained flow reactor.

Biogas species	**Experiment**	**Simulation Isothermal**	**Simulation Nonisothermal**
CO	0.4742 ±0.0045	0.3728	0.3413
CO_2	0.4019 ±0.0046	0.4562	0.5050
CH_4	0.0636 ±0.0005	0.0548	0.0558
C_2H_2	0.0025 ±0.0002	NA	NA
C_2H_4	0.0244 ±0.0007	0.0837	0.0677
C_2H_6	0.0089 ±0.0001	0.0258	0.0210
C_3-C_4	0.0202±0.0016	NA	NA
H_2	0.0042 ±0.0001	0.0066	0.0089

5. Conclusion

A biomass pyrolyzer is a complex multiphase, multiscale system with reacting gas and solid phases, and transport phenomena occur at different time and length scales. Computational fluid

dynamics simulation is an efficient tool for biomass pyrolyzer design, optimization, and scale-up. One of the challenges in biomass pyrolysis simulations is dealing with the kinetic mechanism because of the complex composition and the variability of feedstocks. In this study, a detailed biomass pyrolysis kinetics mechanism was assessed in multiscale simulations of a single particle pyrolyzer and a pilot-scale entrained flow pyrolyzer. A multiscale simulation framework for biomass pyrolyzer was developed by integrating CRECK kinetics, a 1-D particle scale model, and a particle-in-cell reactor model. It is found that the predicted yield and composition of bio-char, bio-oil, and bio-gas are in excellent agreement with single-particle pyrolysis experimental data using the nonisothermal model. However, in the pilot-scale entrained flow pyrolyzer, the isothermal model performed better. Explanations for these results include the possibility of limitations in the CRECK kinetic scheme, or isotropic particle scale assumptions. Further work should be done to explore the impact of anisotropic physical properties on the overall conversion rate for particles under fast pyrolysis conditions. This study provides some insights into biomass pyrolysis kinetics development for a broad range of operating conditions and biomass feedstocks, and pyrolyzer multiscale simulation at different scales in a future study.

Acknowledgement

This work was performed in support of the US Department of Energy's EERE Bioenergy Technologies Office (BETO) as part of the BETO Consortium for Computational Physics and Chemistry (CCPC). The research was executed through the NETL Research and Innovation Center's BETO CCPC. Research performed by Leidos Research Support Team staff was conducted under the RSS contract 89243318CFE000003. Research performed in part by the National Renewable Energy Laboratory, operated by Alliance for Sustainable Energy, LLC, for the U.S. Department of Energy (DOE) under Contract No. DE-AC36-08GO28308. This work was partially

funded by the Deutsche Forschungsgemeinschaft (DFG, German Research Foundation) – Projekt Nummer 215035359 – TRR 129. The authors would like to thank Huda Ashfaq and Bryan Hughes for their help in the biomass characterization.

CRediT author statement

Xi Gao: Software, Formal analysis, Conceptualization, Writing- Original draft preparation. **Liqiang Lu:** Software, Formal analysis, Writing- Original draft preparation. **Mehrdad Shahnam:** Software, Resources. **William A. Rogers:** Conceptualization, Funding acquisition. **Kristin Smith:** Investigation, Formal analysis. **Katherine Gaston:** Investigation, Formal analysis. **David Robichaud:** Conceptualization, Resources, Writing- Reviewing and Editing. **M. Brennan Pecha:** Software, Investigation, Writing- Reviewing and Editing. **Meagan Crowley:** Software, Investigation. **Peter N. Ciesielski:** Conceptualization, Funding acquisition, Writing- Reviewing and Editing. **Paulo Debiagi:** Methodology, Writing- Reviewing and Editing. **Tiziano Faravelli:** Methodology, Writing- Reviewing and Editing, Funding acquisition. **Gavin Wiggins:** Software, Investigation, Writing- Reviewing and Editing. **Charles E.A. Finney:** Software, Resources, Writing- Reviewing and Editing. **James E Parks II:** Conceptualization, Funding acquisition.

Disclaimer

otherwise does not necessarily constitute or imply its endorsement, recommendation, or favoring by the United States Government or any agency thereof. The views and opinions of authors expressed herein do not necessarily state or reflect those of the United States Government or any agency thereof.

This work was authored in part by the National Renewable Energy Laboratory, operated by Alliance for Sustainable Energy, LLC, for the U.S. Department of Energy (DOE) under Contract No. DE-AC36-08GO28308. Funding provided by U.S. Department of Energy Office of Energy Efficiency and Renewable Energy Solar Energy Technologies Office. The views expressed in the article do not necessarily represent the views of the DOE or the U.S. Government. The U.S. Government retains and the publisher, by accepting the article for publication, acknowledges that the U.S. Government retains a nonexclusive, paid-up, irrevocable, worldwide license to publish or reproduce the published form of this work, or allow others to do so, for U.S. Government purposes.

References

[1] A.V. Bridgwater, Review of fast pyrolysis of biomass and product upgrading, Biomass and bioenergy 38 (2012) 68-94.

[2] P.N. Ciesielski, M.B. Pecha, A.M. Lattanzi, V.S. Bharadwaj, M.F. Crowley, L. Bu, J.V. Vermaas, K.X. Steirer, M.F. Crowley, Advances in Multiscale Modeling of Lignocellulosic Biomass, ACS Sustainable Chemistry & Engineering 8 (2020) 3512-3531.

[3] Q. Xiong, K. Hong, F. Xu, J.D. Smith, J. Chaouki, CFD simulation of biomass thermochemical conversion: Model development, practical application and experimental validation, Renewable Energy 147 (2020) 2043–2045.

[4] D. Carpenter, T.L. Westover, S. Czernik, W. Jablonski, Biomass feedstocks for renewable fuel

production: a review of the impacts of feedstock and pretreatment on the yield and product distribution of fast pyrolysis bio-oils and vapors, Green Chemistry 16 (2014) 384-406.

[5] X. Gao, J. Yu, C. Li, R. Panday, Y. Xu, T. Li, H. Ashfaq, B. Hughes, W.A. Rogers, Comprehensive experimental investigation on biomass‐glass beads binary fluidization: A data set for CFD model validation, AIChE Journal 66 (2020) e16843.

[6] L. Lu, J. Yu, X. Gao, Y. Xu, M. Shahnam, W.A. Rogers, Experimental and numerical investigation of sands and Geldart A biomass co‐fluidization, AIChE Journal 66 (2020) e16969.

[7] M.B. Pecha, E. Ramirez, G.M. Wiggins, D. Carpenter, B. Kappes, S. Daw, P.N. Ciesielski, Integrated particle-and reactor-scale simulation of pine pyrolysis in a fluidized bed, Energy & Fuels 32 (2018) 10683-10694.

[8] A.L. Brown, D.C. Dayton, M.R. Nimlos, J.W. Daily, Design and characterization of an entrained flow reactor for the study of biomass pyrolysis chemistry at high heating rates, Energy & Fuels 15 (2001) 1276-1285.

[9] M.S. Bohn, C.B. Benham, Biomass pyrolysis with an entrained flow reactor, Industrial & Engineering Chemistry Process Design and Development 23 (1984) 355-363.

[10] P.N. Ciesielski, M.B. Pecha, V.S. Bharadwaj, C. Mukarakate, G.J. Leong, B. Kappes, M.F. Crowley, S. Kim, T.D. Foust, M.R. Nimlos, Advancing catalytic fast pyrolysis through integrated multiscale modeling and experimentation: Challenges, progress, and perspectives, Wiley Interdisciplinary Reviews: Energy and Environment 7 (2018) e297.

[11] M.-K. Bahng, C. Mukarakate, D.J. Robichaud, M.R. Nimlos, Current technologies for analysis of biomass thermochemical processing: A review, Analytica Chimica Acta 651 (2009) 117-138.

[12] P.E.A. Debiagi, C. Pecchi, G. Gentile, A. Frassoldati, A. Cuoci, T. Faravelli, E. Ranzi, Extractives extend the applicability of multistep kinetic scheme of biomass pyrolysis, Energy &

Fuels 29 (2015) 6544-6555.

[13] A. Anca-Couce, Reaction mechanisms and multi-scale modelling of lignocellulosic biomass pyrolysis, Progress in Energy and Combustion Science 53 (2016) 41-79.

[14] S. Hameed, A. Sharma, V. Pareek, H. Wu, Y. Yu, A review on biomass pyrolysis models: kinetic, network and mechanistic models, Biomass and Bioenergy 123 (2019) 104-122.

[15] M.B. Pecha, J.I.M. Arbelaez, M. Garcia-Perez, F. Chejne, P.N. Ciesielski, Progress in understanding the four dominant intra-particle phenomena of lignocellulose pyrolysis: chemical reactions, heat transfer, mass transfer, and phase change, Green chemistry 21 (2019) 2868-2898.

[16] H.B. Mayes, L.J. Broadbelt, Unraveling the reactions that unravel cellulose, The Journal of Physical Chemistry A 116 (2012) 7098-7106.

[17] A.K. Burnham, X. Zhou, L.J. Broadbelt, Critical review of the global chemical kinetics of cellulose thermal decomposition, Energy & Fuels 29 (2015) 2906 -2918.

[18] E. Ranzi, M. Corbetta, F. Manenti, S. Pierucci, Kinetic modeling of the thermal degradation and combustion of biomass, Chemical Engineering Science 110 (2014) 2-12.

[19] T. Faravelli, A. Frassoldati, E.B. Hemings, E. Ranzi, Multistep Kinetic Model of Biomass Pyrolysis, Cleaner Combustion, Springer2013, pp. 111-139.

[20] P. Debiagi, T. Faravelli, C. Hasse, E. Ranzi, Kinetic Modeling of Solid, Liquid and Gas Biofuel Formation from Biomass Pyrolysis, Production of Biofuels and Chemicals with Pyrolysis, Springer2020, pp. 31-76.

[21] P. Debiagi, G. Gentile, A. Cuoci, A. Frassoldati, E. Ranzi, T. Faravelli, A predictive model of biochar formation and characterization, Journal of Analytical and Applied Pyrolysis 134 (2018) 326-335.

[22] M. Corbetta, A. Frassoldati, H. Bennadji, K. Smith, M.J. Serapiglia, G. Gauthier, T. Melkior,

E. Ranzi, E.M. Fisher, Pyrolysis of centimeter-scale woody biomass particles: kinetic modeling and experimental validation, Energy & fuels 28 (2014) 3884-3898.

[23] M.S. Mettler, D.G. Vlachos, P.J. Dauenhauer, Top ten fundamental challenges of biomass pyrolysis for biofuels, Energy & Environmental Science 5 (2012) 7797-7809.

[24] G.M. Wiggins, P.N. Ciesielski, C.S. Daw, Low-order modeling of internal heat transfer in biomass particle pyrolysis, Energy & Fuels 30 (2016) 4960-4969.

[25] M.B. Pecha, M. Garcia-Perez, T.D. Foust, P.N. Ciesielski, Estimation of heat transfer coefficients for biomass particles by direct numerical simulation using microstructured particle models in the laminar regime, ACS Sustainable Chemistry & Engineering 5 (2017) 1046-1053.

[26] L. Lu, X. Gao, M. Shahnam, W.A. Rogers, Open Source Implementation of Glued Sphere Discrete Element Method and Non‐spherical Biomass Fast Pyrolysis Simulation, AIChE Journal e17211.

[27] L. Lu, X. Gao, M. Shahnam, W.A. Rogers, Bridging particle and reactor scales in the simulation of biomass fast pyrolysis by coupling particle resolved simulation and coarse grained CFD-DEM, Chemical Engineering Science 216 (2020) 115471.

[28] K. Papadikis, S. Gu, A. Bridgwater, CFD modelling of the fast pyrolysis of biomass in fluidised bed reactors. Part B: Heat, momentum and mass transport in bubbling fluidised beds, Chemical Engineering Science 64 (2009) 1036-1045.

[29] X. Gao, J. Yu, L. Lu, W.A. Rogers, Coupling particle scale model and SuperDEM‐CFD for multiscale simulation of biomass pyrolysis in a packed bed pyrolyzer, AIChE Journal e17139.

[30] X. Gao, J. Yu, R.J. Portal, J.-F. Dietiker, M. Shahnam, W.A. Rogers, Development and validation of SuperDEM for non-spherical particulate systems using a superquadric particle method, Particuology (2021).

[31] X. Gao, J. Yu, L. Lu, C. Li, W.A. Rogers, Development and validation of SuperDEM-CFD coupled model for simulating non-spherical particles hydrodynamics in fluidized beds, Chemical Engineering Journal (2020) 127654.

[32] M. Syamlal, W. Rogers, T.J. O'Brien, MFIX documentation: Theory guide, National Energy Technology Laboratory, Department of Energy, Technical Note DOE/METC-95/1013 and NTIS/DE95000031 (1993).

[33] L. Lu, X. Gao, A. Gel, G.M. Wiggins, M. Crowley, B. Pecha, M. Shahnam, W.A. Rogers, J. Parks, P.N. Ciesielski, Investigating biomass composition and size effects on fast pyrolysis using global sensitivity analysis and CFD simulations, Chemical Engineering Journal (2020) 127789.

[34] M.A. Clarke, J.M. Musser, The MFiX Particle-in-Cell Method (MFiX-PIC) Theory Guide, NETL, 2020.

[35] R. Garg, J. Dietiker, Documentation of open-source MFIX–PIC software for gas-solids flows, From URS https://mfix. netl. doe. gov/documentation/mfix_pic_doc. pdf (2013).

[36] Y. Xu, X. Gao, T. Li, Numerical study of the bi-disperse particles segregation inside a spherical tumbler with Discrete Element Method (DEM), Computers & Mathematics with Applications (2019).

[37] J. Li, W. Ge, W. Wang, N. Yang, X. Liu, L. Wang, X. He, X. Wang, J. Wang, M. Kwauk, From multiscale modeling to meso-science, Springer2013.

[38] H. Pan, X.-Z. Chen, X.-F. Liang, L.-T. Zhu, Z.-H. Luo, CFD simulations of gas–liquid–solid flow in fluidized bed reactors—A review, Powder Technology 299 (2016) 235-258.

[39] M.J. Andrews, P.J. O'Rourke, The multiphase particle-in-cell (MP-PIC) method for dense particulate flows, International Journal of Multiphase Flow 22 (1996) 379-402.

[40] G.H. Ganser, A rational approach to drag prediction of spherical and nonspherical particles,

Powder Technology 77 (1993) 143-152.

[41] R. Di Felice, The voidage function for fluid-particle interaction systems, International Journal of Multiphase Flow 20 (1994) 153-159.

[42] L. Lu, X. Gao, M. Shahnam, W.A. Rogers, Coarse grained computational fluid dynamic simulation of sands and biomass fluidization with a hybrid drag, AIChE Journal 66 (2020) e16867.

[43] H. Tavassoli, E.A.J.F. Peters, J.A.M. Kuipers, Direct numerical simulation of fluid – particle heat transfer in fixed random arrays of non-spherical particles, Chemical Engineering Science 129 (2015) 42-48.

[44] D.J. Gunn, Transfer of heat or mass to particles in fixed and fluidised beds, International Journal of Heat and Mass Transfer 21 (1978) 467-476.

[45] A. Anca-Couce, P. Sommersacher, R. Scharler, Online experiments and modelling with a detailed reaction scheme of single particle biomass pyrolysis, Journal of Analytical and Applied Pyrolysis 127 (2017) 411-425.

[46] K. Gaston, K. Smith, Integration & Scale-Up Q3 Milestone Report, National Renewable Energy Laboratory, Department of Energy (2017).

[47] X. Gao, T. Li, W.A. Rogers, K. Smith, K. Gaston, G. Wiggins, J.E. Parks II, Validation and application of a multiphase CFD model for hydrodynamics, temperature field and RTD simulation in a pilot-scale biomass pyrolysis vapor phase upgrading reactor, Chemical Engineering Journal (2020) 124279.

[48] K.M. Smith, K.R. Gaston, Effect of Blended Feedstock on Pyrolysis Oil Composition, National Renewable Energy Lab.(NREL), Golden, CO (United States),Report NREL/PO-5100-70131, 2017.

[49] X. Gao, T. Li, A. Sarkar, L. Lu, W.A. Rogers, Development and validation of an enhanced

filtered drag model for simulating gas-solid fluidization of Geldart A particles in all flow regimes, Chemical Engineering Science 184 (2018) 33-51.

[50] J.F. Dietiker, Multiphase Flow with Interphase eXchanges Cartesian Grid User Guide, National Energy Technology Laboratory (from) (2013).

[51] G. Gentile, P.E.A. Debiagi, A. Cuoci, A. Frassoldati, E. Ranzi, T. Faravelli, A computational framework for the pyrolysis of anisotropic biomass particles, Chemical Engineering Journal 321 (2017) 458-473.

[52] G.L. Comstock, Directional permeability of softwoods, Wood and Fiber Science 1 (1970) 283-289.

[53] P.N. Ciesielski, M.F. Crowley, M.R. Nimlos, A.W. Sanders, G.M. Wiggins, D. Robichaud, B.S. Donohoe, T.D. Foust, Biomass particle models with realistic morphology and resolved microstructure for simulations of intraparticle transport phenomena, Energy & Fuels 29 (2015) 242-254.

Graphical abstract

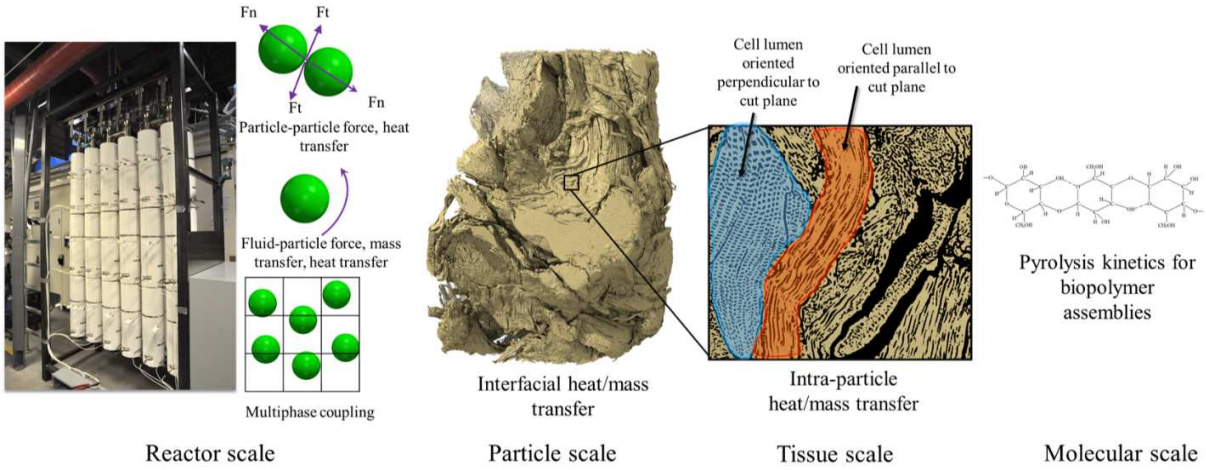

Figure 1. A multiscale simulation framework for a biomass pyrolyzer by integrating a detailed pyrolysis kinetic mechanism, a particle-scale model, and a reactor-scale model.